DOI: https://doi.org/10.2138/am-2020-7361

Revision 2

A new occurrence of corundum in eucrite and its significance

Jie-Ya Li[1], Ai-Cheng Zhang[1,2,*], Naoya Sakamoto[3], Hisayoshi Yurimoto[3,4,5], Li-Xin Gu[6]

[1] State Key Laboratory for Mineral Deposits Research, School of Earth Sciences and Engineering, Nanjing University, Nanjing 210023 China

[2] CAS Center for Excellence in Comparative Planetology, China

[3] Isotope Imaging Laboratory, Creative Research Institution, Hokkaido University, Sapporo 010-0021, Japan

[4] Department of Natural History Sciences, Hokkaido University, Sapporo 060-0810, Japan

[5] Institute of Space and Astronautical Science, Japan Aerospace Exploration Agency, Kanagawa 252-5210, Japan

[6] Institute of Geology and Geophysics, Chinese Academy of Sciences, Beijing 100029, China

*Corresponding author. Ai-Cheng Zhang, e-mail: aczhang@nju.edu.cn

Jie-Ya Li, e-mail: 1403219034@qq.com

Naoya Sakamoto, e-mail: naoya@ep.sci.hokudai.ac.jp

Hisayoshi Yurimoto, e-mail: yuri@ep.sci.hokudai.ac.jp

Li-Xin Gu, e-mail: gulixin@mail.iggcas.ac.cn

For submission to ***American Mineralogist***

ABSTRACT

Diversity of lithologies is an important proxy of internal evolution in differentiated planets and asteroids. The major lithologies in Vesta, based on the howardite-eucrite-diogenite clan meteorites, include basalt, gabbro, noritic orthopyroxenite, orthopyroxenite, dunite, harzburgite, and dacite. No other lithology has been reported up to date. In this study, we report a new occurrence of corundum in eucrite meteorite Northwest Africa (NWA) 8647. Three-dimensional petrographic observations reveal that the corundum grain occurs as a mineral inclusion in highly deformed pyroxene fragment. The texture indicates that the corundum is not a contaminant. The corundum-associated pyroxenes have Fe-Mn compositions consistent with typical pyroxenes from howardite-eucrite-diogenite meteorites. We suggest that the corundum grain could be an xenocryst incorporated during the ascent of a basaltic magma. The results might indicate the presence of an Al-rich, Si-poor region, probably lithology in the interior of Vesta, implying that the evolution and internal structure should be much more complex than previously thought.

Keywords: corundum; Northwest Africa 8647, Al-rich lithology; eucrite; Vesta

INTRODUCTION

The magma ocean concept is one of the most fundamental hypotheses in Earth and planetary Sciences. In magma ocean models, differentiated celestial bodies have experienced a global melting and differentiation after accretion. The magma ocean phase has been considered as the starting point for most of the differentiated planets and asteroids (Elkins-Tanton, 2012). However, records of the magma ocean phase in the terrestrial planets (such as Earth and Mars) are extremely rarely preserved due to later complex processes including plate tectonics and weathering. One of the methods of constraining the earliest evolution of the terrestrial planets may rely on the investigations of differentiated protoplanets, in which the records of early stage evolution have been largely preserved (Zuber et al., 2011).

Asteroid 4 Vesta is the largest known protoplanet in our solar system with a core-mantle-crust structure (Russell et al., 2012) and its differentiation might have taken place a few million years after the formation of the earliest solid material in the solar system (Wadhwa et al., 2009). Therefore, Vesta plays an important role in understanding early processes and evolution of terrestrial planets. Meanwhile, the differentiation and evolution of Vesta can be constrained based on the diversity and origin of lithologies found in meteorite samples from Vesta and the remote-sensing data of Vesta. In the past decades, many investigations have been performed on howardite-eucrite-diogenite (HED) meteorites, the samples that have likely been derived from Vesta (Mittlefehldt, 2015). The lithologies that have been reported in HED meteorites include basalt, gabbro, noritic orthopyroxenite, orthopyroxenite, dunite, harzburgite, and dacite (e.g., Beck and

DOI: https://doi.org/10.2138/am-2020-7361

McSween, 2010; McSween et al., 2011; Mittlefehldt, 2015; Hahn et al., 2017; Zhang et al., 2020).

Corundum is an important mineral indicator of Al-rich compositions for terrestrial rocks (Giuliani et al., 2014). In HED meteorites, it was only reported as a shock-induced mineral in the eucrite Northwest Africa 8003 (Pang et al., 2018, 2019). Recently, during investigation of shock-metamorphism in HED meteorites, a corundum grain was observed as an inclusion in pyroxene in the Northwest Africa (NWA) 8647 eucrite. Its occurrence is different from other extraterrestrial occurrences of corundum including that was described in Pang et al. (2018, 2019). In this study, we report its occurrence, identification, and potential significance for a hidden Al-rich, Si-poor region in the interior of Vesta.

ANALYTICAL METHODS

The polished section of the NWA 8647 used in this study was prepared in the following sequence. First, a thin chip of NWA 8647 was cut with diamond blade and attached on a 1-inch rounded silica slide with epoxy. Then, the sample was thinned to approximately 0.1 mm in thickness with SiC abrasive papers. After that, the sample was polished with diamond pastes of various particle sizes (5 μm, 1 μm, and 0.5 μm). During the whole process of sample preparation, no alumina polishing paste was used. Before being observed with the scanning electron microscope (SEM), the sample was carbon coated.

Petrographic textures in the meteorite NWA 8647 were observed using a Zeiss Supra 55 scanning electron microscope under backscattering electron (BSE) mode at Nanjing University, Nanjing, China. An energy dispersive spectrometer (EDS) installed on this SEM instrument was used to qualitatively identify mineral phases in the polished section. Quantitative mineral chemical analyses were obtained by wavelength dispersive spectrometers installed in a JEOL 8100 electron probe microanalyzer (EPMA) at Nanjing University. An accelerating voltage of 15 kV was used. The EPMA analysis with a beam current of 20 nA was carried out for most minerals in this study. Measurement times are 20 s for peaks and 10 s for background, respectively. Natural and synthetic standards were used for concentration calibration. All data were reduced with the ZAF (atomic number-absorption-fluorescence) procedure.

The structural identification of corundum and surrounding minerals was performed using an electron backscatter diffraction detector (EBSD) attached on the JEOL 7000F field emission SEM instrument at Hokkaido University, Sapporo, Japan. Before the EBSD analyses, the sample was vibro-polished with silica suspension and carbon coated. The EBSD pattern and EDS pattern of minerals were obtained simultaneously with the Aztec software. An accelerating voltage of 20 kV and a beam current of 4 nA were used. The EBSD patterns of corundum were indexed with various polymorphs of Al_2O_3. The Aztec software automatically suggests indexing solutions ranked by the lowest "mean angular deviation" (MAD) as an index of "goodness of fit." MAD numbers <1 are considered desirable for accurate solutions (Ma and Rossman, 2008; Zhang et al., 2015).

To constrain the textural relationship between corundum and surrounding materials in three dimensions, an ultrathin section was cut through the corundum grain perpendicular to the thin section surface using the focused ion beam (FIB) technique at the Institute of Geology and Geophysics, Chinese Academy of Sciences, Beijing. The FIB milling was conducted on a Zeiss Auriga Compact SEM instrument. A focused Gaion beam which was accelerated under various high voltages (4–30 kV) was used to sputter material from the sample. Before fine milling, a few secondary electron images of the ultrathin section were made at an accelerating voltage of 1.5–5 kV. After that, the ultrathin section was mapped with SEM-EDS at a 10-kV accelerating voltage. The final section is approximately 100 nm in thickness. Unfortunately, the ultrathin section was lost from the Cu grid before observation with transmission electron microscope.

RESULTS

The NWA 8647 meteorite is a 326-gram brecciated eucrite (Bouvier et al., 2017). The polished section of NWA 8647 used in this study contains two petrographically different portions (Fig. 1). In one portion, the sample was largely melted and recrystallized. However, lithic fragments and pyroxene, plagioclase, and silica mineral fragments are commonly observed in this portion. In the fine-grained, melted and recrystallized region, pyroxene and plagioclase form a fine-grained, subophitic texture, in which pyroxene grains have a large chemical variation ($En_{12.9–59.9}Fs_{31.9–61.2}Wo_{8.3–26.7}$) with a Fe/Mn value of 23–32 (Table S1, Figs. 2–3). The composition of plagioclase is $An_{87.2–91.3}Ab_{8.4–12.6}Or_{0.2–0.3}$ (Table S2).

The other portion of the polished section was not melted and has a complex petrographic texture (Fig. 1). A few shock-induced melt veins are present in this unmelted portion (Fig. 1). The shock-induced melt veins are composed mainly of fine-grained clinopyroxene grains with cation vacancies (compositions are not given in the present paper). No other high-pressure phases have been observed in this meteorite. Some unmelted regions show a coarse-grained, ophitic-subophitic texture of pyroxene and plagioclase, in which pyroxene usually contains exsolution lamellae (up to 25 μm in width, Fig. 4). Both low-Ca pyroxene and high-Ca pyroxene with exsolution texture have limited compositional variations, $En_{36.3–39.2}Fs_{57.3–61.1}Wo_{1.8–4.4}$ and $En_{29.4–30.9}Fs_{25.1–27.8}Wo_{42.2–44.6}$, respectively (Fig. 2). The Fe-Mn compositions of the coarse-grained pyroxenes (especially low-Ca pyroxene) plot along the trend line for HED meteorites (Fig. 3; Papike et al., 2003). The mean compositions of the coarse-grained low-Ca pyroxene and high-Ca pyroxene with exsolution texture are $En_{37.7}Fs_{59.5}Wo_{2.8}$ and $En_{30.0}Fs_{26.6}Wo_{43.4}$, respectively, suggesting a two-pyroxene equilibrium temperature at 816 ^{o}C with the assumption of a pressure at 10 kbar (Brey and Köhler, 1990). The plagioclase compositions are $An_{87.4–90.5}Ab_{9.3–12.2}Or_{0.2–0.5}$ (Table S2).

The corundum grain in NWA 8647 is observed in a large pyroxene fragment (~280 μm in size), which is located in the fine-grained melted and recrystallized portion of NWA 8647 (Figs. 1 and 5a). This pyroxene fragment has been largely affected by shock metamorphism. The major part of the pyroxene fragment has deformed and transformed into fine-grained pyroxene grains approximately 1–2 μm size. However, high-Ca pyroxene exsolution lamellae ($En_{33.7–35.0}Fs_{26.3–29.2}Wo_{36.3–40.0}$) can be still recognized within low-Ca pyroxene ($En_{40.8–43.5}Fs_{47.8–54.9}Wo_{2.7–10.9}$). The Fe-Mn compositions of the pyroxenes plot on the trend line for HED meteorites (Fig. 3). However, in the pyroxene quadrilateral diagram, the pyroxenes associated with the corundum grain plot slightly to the Mg-rich side of the coarse-grained pyroxenes in the unmelted regions (Fig. 2). Moreover, the low-Ca pyroxene in the fragment associated with corundum is also slightly Ca-enriched compared to the coarse-grained low-Ca pyroxene in unmelted portion; whereas the high-Ca pyroxene in the fragment associated with corundum is also slightly Ca-depleted compared with the coarse-grained high-Ca pyroxene in the unmelted portion

(Fig. 2). Fine-grained polycrystalline chromite is also present as inclusions in the pyroxene fragment (Fig. 5b).

The corundum grain is triangular in shape and approximately 4 μm in its largest dimension (Fig. 5c). The EPMA results reveal it contains dominant Al_2O_3 (98.1–98.5 wt%) with minor SiO_2 (0.53–0.55 wt%) and FeO (1.15–1.18 wt%), which might be due to beam-overlapping on surrounding pyroxene. The corundum grain is in tight contact with the host pyroxene grain in the thin-section plane and the plane perpendicular to the thin-section surface (Figs. 5c and 6). Based on the high-magnification SEM image of the FIB section, a few tiny, anhedral plagioclase grains (<0.6 μm in length) are associated with the pyroxene (Fig. 6); however they are not in direct contact with the corundum grain. Structure of the corundum grain is confirmed based on its EBSD pattern, which is best indexed with the $R\overline{3}c$ corundum structure (MAD=0.21; Fig. 7) and cannot be indexed with other Al_2O_3 phases. The crystal structure of the pyroxene fragment including the corundum grain was also confirmed with EBSD patterns.

To understand a potential reason why the pyroxene fragment including corundum has compositions different from the coarse-grained pyroxene in the unmelted portion, compositions of polycrystalline pyroxenes in a large lithic fragment (Fig. 8), also located in the melted and recrystallized portion, were also measured with EPMA (Table S1). The polycrystalline pyroxenes have a grain size varying from 5 to 10 μm and show Z-contrast heterogeneity in the BSE image. Some relatively large grains show a bright-dark-bright zoning texture from the core to the rim (Fig. 8b). The rims of pyroxene grains were not measured to avoid potential overlapping on surrounding plagioclase. At the interface between pyroxene and plagioclase, plagioclase usually occurs as thin lath-like crystals

(Fig. 8b). Measurements on the pyroxene grains show a Fe-Mn compositional variation consistent with the trend line for HED meteorites (Fig. 3), while these pyroxenes plot with a large variation slightly to the Mg-rich side of the coarse-grained pyroxenes from the unmelted portion, but to the Fe-rich side of the pyroxene fragment including corundum in the pyroxene quadrilateral diagram (Fig. 2).

DISCUSSION

Corundum is usually used as a polishing material for sample preparation in many laboratories. In addition, corundum can exist in many terrestrial rocks. Therefore, we are very cautious about the source of the corundum grain in our sample. During the whole sample preparation processes in our laboratory, no alumina powder was used. Only SiC and diamond were used as polishing materials. This would largely decrease the possibility that the corundum grain was a contaminant during sample preparation. Importantly, the corundum grain is in tight contact with the host pyroxene in three dimensions based on the observations on the thin-section plane and the FIB-section plane. This feature is different from the occurrences of polishing paste contaminants in the literature (e.g., Dobrzhintskaya et al., 2014). Therefore, the possibility that the corundum grain in NWA 8647 was contamination during sample preparation can be excluded.

Corundum is also an important phase in chondritic meteorites, as presolar grains (e.g., Takigawa et al., 2018 and references therein) and as a primary or secondary phase in Ca,Al-rich inclusions (e.g., Simon et al., 2002; Ma et al., 2009; Makide et al., 2009, 2013 and references therein). Exotic chondritic fragments have usually been observed in brecciated HED meteorites (e.g., Zolensky et al., 1996; Lorenz et al., 2007; and references therein). This imposes a possibility that the corundum grain and its associated pyroxenes were derived from other asteroids rather than the eucrite parent body. However, the occurrence of corundum in NWA 8647 is largely distinct from those of chondritic corundum. For instance, presolar grains in chondrites are much smaller than the corundum grain and usually occur as discrete grains in the fine-grained matrix in chondrites (Zinner, 2014). Therefore, it is reasonable to consider that presolar corundum grains might also occur mainly as discrete grains. The primary and secondary corundum grains in Ca,Al-rich inclusions are usually associated with other primary or secondary Ca,Al-rich minerals (e.g., melilite, grossular, nepheline; Simon et al., 2002; Ma et al., 2009; Makide et al., 2009, 2013 and references therein). However, in the current study, corundum appears totally enclosed in pyroxenes in three dimensions. Furthermore, the corundum-associated pyroxene grains in NWA 8647 show an exsolution texture, which is absent in chondritic materials. Importantly, the corundum-associated pyroxene fragment in NWA 8647 have a Fe-Mn compositional variation well consistent with typical HED pyroxenes (Fig. 3). Therefore, the corundum grain and its associated pyroxenes are not exotic chondritic fragment. Instead, they were probably derived from the eucrite parent body.

The major element compositions of the corundum-associated pyroxene fragment in NWA 8647 are slightly different from those of the coarse-grained pyroxenes in the unmelted portion (Fig. 2). This deviation can be explained if the corundum-associated pyroxenes had a source different from the other pyroxenes in NWA 8647. Alternatively, the compositional deviation might be due to elemental exchange with the surrounding melt during and after the melting and recrystallization of the sample. Similar textural and chemical features have been observed for olivine and chromite in shocked lunar meteorites and some shocked eucrites (e.g., Zhang et al., 2011; Pang et al., 2017). During the shock-induced melting, the pyroxene fragment was highly deformed and many pyroxene grains approximately 1–2 μm in size formed. The small pyroxene sub-grains might have exchanged Mg, Fe, and Ca with surrounding melt. During shock-induced high temperature and fast cooling, Mg would be preferably incorporated into pyroxene structure, which can account for why the compositions of the pyroxene fragment including corundum plot to the Mg-rich side of the coarse-grained pyroxenes in the unmelted portion (Fig. 2). Presence of the tiny plagioclase grains shown in Fig. 6 might indicate that high-temperature melt migrated into the grain boundaries between fine-grained pyroxenes in the fragment, although such tiny grains cannot be recognized at low-magnification BSE images. Such an interpretation is generally supported by the compositional deviation of the polycrystalline pyroxenes in the lithic fragment shown in Fig. 8 from the coarse-grained pyroxenes in the unmelted portion (Fig. 2). The pyroxene grains shown in Fig. 8b have a grain size of 5–10 μm, larger than the pyroxene grains in the fragment including corundum. The large grain size might only allow for limited elemental exchange, which can account for why the pyroxene grains shown in Fig. 8b plot only slightly to the Mg-rich size of the coarse-grained pyroxene in the unmelted portion (Fig. 2).

Corundum has been observed in the eucrite NWA 8003 (Pang et al., 2018, 2019). The corundum in NWA 8003 occurs as micron to submicron euhedral grains associated with ilmenite, vacancy-rich clinopyroxene, vestaite, and kyanite only in shock-induced melt pockets, which are usually surrounded by tissintite (Pang et al., 2019). No corundum grains were observed in the host rock of NWA 8003. Pang et al. (2019) interpreted the corundum in NWA 8003 to be one of the crystallization products after partial melting involving ilmenite, pyroxene, plagioclase, and silica under high pressures. Recently, Yang et al. (2019) described the presence of corundum in the ungrouped achondrite NWA 7325. The corundum in NWA 7325 occurs as needle-like crystals (<0.9 μm in length) in the interior of large plagioclase (Yang et al., 2019). The authors suggested that the corundum might have crystallized from molten plagioclase, which can be accounted for by the melting reaction of anorthite at high temperature (Goldsmith, 1980). In the present study, although the corundum-associated pyroxenes are polycrystalline in texture, probably due to shock metamorphism and its heating effect, no melting reaction similar to those in NWA 8003 and NWA 7325 was observed in NWA 8647. The corundum-associated mineral assemblage in NWA 8647 is distinctly different from those of shock-induced corundum in NWA 8003. Although minor plagioclase grains have been observed in the pyroxene fragment including corundum in NWA 8647, the grain sizes of these plagioclase grains are much smaller than the corundum. Corundum was also not observed in other regions in NWA 8647. Based on the current observations, the corundum grain in NWA 8647 cannot be a product of shock metamorphism in the host rock. Instead, the corundum grain in NWA 8647 is most likely be of indigenous origin.

Our observations reveal that the corundum grain in the current study could be a mineral inclusion in orthopyroxene with augite exsolution lamellae. During shock metamorphism of NWA 8647, deformation and polycrystallization took place in the pyroxenes, with the corundum grain not heavily affected. Given that eucritic melts are not corundum-normative (Stolper, 1975), the corundum grain in NWA 8647 was probably captured as an xenocryst during the ascent of a basaltic magma and included by a pyroxene grain that has crystallized from the basaltic melt. This origin might be similar to the corundum in terrestrial alkali basaltic extrusions (e.g., Guo et al., 1996; Sutherland et al., 1998).

Natural corundum has been widely observed in a variety of terrestrial lithologies (e.g., Giuliani et al., 2014) and primitive chondrites (e.g., Simon et al., 2002; Makide et al., 2013; Takigawa et al., 2018). In terrestrial magmatic rocks, it was observed from syenites and nepheline syenites (e.g., Moyd, 1949), to quartz-free pegmatites (e.g., Rao et al., 2012), porphyry copper deposits (e.g., Bottril, 1998), to alkali basaltic extrusions (e.g., Guo et al., 1996; Sutherland et al., 1998), alkaline basic lamprophyre (e.g., Brownlow and Komorowski, 1988), and kimberlites (e.g., Mazzone and Haggerty, 1989). In the latter three types of occurrence, corundum occurs usually as xenocrysts or in xenoliths. In addition, corundum has also been observed in a variety of high-grade metamorphic aluminous rocks (c.f., Giuliani et al., 2014). In primitive chondrites, corundum grains occur either as presolar grains in fine-grained matrix (e.g., Takigawa et al., 2018) or as a component in Ca-Al-rich inclusions (e.g., Simon et al., 2002; Makide et al., 2013). Although these natural rocks and objects containing corundum vary largely in lithology, their common characteristic is Al-rich and Si-poor, at least locally (Giuliani et al., 2014). Therefore, the occurrence of corundum in NWA 8647 might indicate the presence of an Al-rich and Si-poor region, probably lithology locally in the interior of Vesta, although the exact location of the Al-rich and Si-poor region/lithology remains unconstrained based on the current observations.

IMPLICATIONS

No Al-rich and Si-poor rocks containing corundum have been identified and considered in previous investigations on HED meteorites (c.f., McSween et al., 2011; Mittlefehldt, 2015) and theoretical simulations (Righter and Drake, 1997; Ruzicka et al., 1997; Mandler and Elkins-Tanton, 2013). The finding of a hidden Al-rich and Si-poor region based on the presence of the indigenous corundum in NWA 8647 indicates that the internal evolution of Vesta is more complex than previously thought. In future, more detailed petrographic and mineralogical observations on HED meteorites are needed to further understand the internal evolution and crystallization history of Vesta.

ACKNOWLEDGEMENTS

This work was financially supported by grants from Natural Science Foundation of China (41673068, 41973061) and Natural Science Foundation of Jiangsu Province of China (BK20170017). We appreciate the constructive comments from Jinping Hu and Jin Zhang, and Associate Editor Steve Simon, and from Chi Ma, David W. Mittlefehldt, and an anonymous reviewer on an early version.

REFERENCES

Beck, A.W., and McSween, H.Y. (2010) Diogenites as polymict breccias composed of orthopyroxenite and harzburgite. Meteoritics & Planetary Science, 45, 850–872.

Botrill, R.S. (1998) A corundum-quartz assemblage in altered volcanic rocks, Bond Range, Tasmania. Mineralogical Magazine, 62, 325–332.

Bouvier, A., Gattacceca, J., Agee, C., Grossman, J., and Metzler, K. (2017) The Meteoritical Bulletin, No. 104. Meteoritics & Planetary Science, doi: 10.1111/maps.12930.

Brey, G.P., and Kohler, T. (1990) Geothermobarometry in four-phase lherzolites II. New thermobarometers, and practical assessment of existing thermobarometers. Journal of Petrology, 31, 1353–1378.

Brownlow, A.H., and Komorowski, J.C. (1988) Geology and origin of the Yogo sapphire deposit, Montana. Economic Geology, 83, 875–880.

Dobrzhinetskaya, L., Wirth, R., and Green, H. (2014) Diamonds in Earth's oldest zircons from Jack Hills conglomerate, Australia, are contamination. Earth and Planetary Science Letters, 387, 212–218.

Elkins-Tanton, L.T. (2012) Magma oceans in the inner solar system. Annual Review of Earth and Planetary Sciences, 40, 113–139.

Giuliani, G., Ohnenstetter, D., Fallick, A.E., Groat, L., and Fagan, A.J. (2014) Chapter 2: The geology and genesis of gem corundum deposits. In Geology of gem deposits (Second Edition), edited by Groat L. A. Mineralogical Association of Canada Short Course 44, Tucson AZ. Pp. 29–112.

Goldsmith, J.R. (1980) The melting and breakdown reactions of anorthite at high pressures and temperatures. American Mineralogist, 65, 272–284.

Guo, J., O'Reilly, S.Y., and Griffin, W.L. (1996) Corundum from basaltic terrains: a mineral inclusion approach to the enigma. Contributions to Mineralogy and Petrology, 122, 368–386.

Hahn, T.M., Lunning, N.G., McSween, H.Y., Bodnar, R.J., and Taylor L.A. (2017) Dacite formation on Vesta: Partial melting of the eucritic crust. Meteoritics & Planetary Science, 52, 1173–1196

Ma, C., and Rossman, G.R. (2008) Barioperovskite, $BaTiO_3$, a new mineral from the Benitoite Mine, California. American Mineralogist, 93, 154–157.

Ma, C., Simon, S.B., Rossman, G.R., and Grossman, L. (2009) Calcium Tschermak's pyroxene, $CaAlAlSiO_6$, from the Allende and Murray meteorites: EBSD and micro-Raman characterizations. American Mineralogist, 94, 1483–1486.

Makide, K., Nagashima, K., Krot, A.N., and Huss, G.R. (2009) Oxygen isotopic components of solar corundum grains. The Astrophysical Journal, 706, 142–147.

Makide, K., Nagashima, K., Krot, A.N., Huss, G.R., Hutcheon, I.D., Hellebrand, E., and Petaev, M.I. (2013) Heterogeneous distribution of ^{26}Al at the birth of the solar System: Evidence from corundum-bearing refractory inclusions in carbonaceous chondrites. Geochimica et Cosmochimica Acta, 110, 190–215.

Mandler, B.E., and Elkins-Tanton, L.T. (2013) The origin of eucrites, diogenites, and olivine diogenites: Magma ocean crystallization and shallow magma chamber processes on Vesta. Meteoritics & Planetary Science, 48, 2333–2349.

Mazzone, P., and Haggerty, S.E. (1989) Peraluminous xenoliths in kimberlite: metamorphosed retites produced by partial melting of pelites. Geochimica et Cosmochimica Acta, 53, 1551–1561.

McSween, H.Y., Mittlefehldt, D.W., Beck, A.W., Mayne, R.G., and McCoy, T.J. (2011) HED meteorites and their relationship to the geology of Vesta and the Dawn mission. Space Science Review, 163, 141–174.

Mittlefehldt, D.W. (2015) Asteroid (4) Vesta: I. The howardite-eucrite-diogenite (HED) clan of meteorites. Chemie der Erde, 75, 155–183.

Moyd, L. (1949) Petrology of the nepheline and corundum rocks of southeastern Ontario. American Mineralogist, 34, 736–751.

Neumann, W., Breuer, D., and Spohn, T. (2014) Differentiation of Vesta: implications for a shallow magma ocean. Earth and Planetary Science Letters, 395, 267–280.

Pang, R.L., Zhang, A.C., Wang, S.Z., Wang, R.C., and Yurimoto, H. (2016) High-pressure minerals in eucrite suggest a small source crater on Vesta. Scientific Reports, 6, 26063.

Pang, R.L., Zhang, A.C., and Wang, R.C. (2017) Complex origins of silicate veinlets in HED meteorites: A case study of Northwest Africa 1109. Meteoritics & Planetary Science, 52, 2113–2131.

Pang, R.L., Harries, D., Pollok, K., Zhang, A.C., and Langenhorst, F. (2018) Vestaite, $(Ti^{4+}Fe^{2+})Ti^{4+}{}_3O_9$, a new mineral in the shocked eucrite Northwest Africa 8003. American Mineralogist, 103, 1502–1511.

Pang, R.L., Harries, D., Pollok, K., Zhang, A.C., and Langenhorst, F. (2019) Unique mineral assemblages of shock-induced titanium-rich melt pockets in eucrite Northwest Africa 8003. Geochemistry, in press. https://doi.org/10.1016/j.chemer.2019.125541.

Papike, J.J., Karner, J.M., and Shearer, C.K. (2003) Determination of planetary basalt parentage: A simple technique using the electron microprobe. American Mineralogist, 88, 469–472.

Rao, C., Wang, R.C., Zhang, A.C., and Hu, H. (2012) The corundum + tourmaline nodules related to hydrothermal alteration of spodumene in the Nanping No. 31

pegmatite dyke, Fujian Province, Southeastern China. The Canadian Mineralogist, 50, 1623–1635.

Righter, K., and Drake, M.J. (1997) A magma ocean on Vesta: core formation and petrogenesis of eucrites and diogenites. Meteoritics & Planetary Science, 32, 929–944.

Ruzicka, A., Snyder, G.A., and Taylor, L.A. (1997) Vesta as the howardite, eucrite and diogenite parent body: implications for the size of a core and for large-scale differentiation. Meteoritics & Planetary Science, 32, 825–840.

Russell, C.T., Raymond, C.A., Coradini, A., McSween, H.Y., Zuber, M.T., Nathues, A., De Sanctis, M.C., Jaumann, R., Konopliv, A.S., Preusker, F., Asmar, S.W., Park, R.S., Gaskell, R., Keller, H.U., Mottola, S., Roatsch, T., Scully, J.E.C., Smith, D.E., Tricarico, P., Toplis, M.J., Christensen, U.R., Feldman, W.C., Lawrence, D.J., McCoy, T.J., Prettyman, T.H., Reedy, R.C., Sykes, M.E., and Titus, T.H. (2012) Dawn at Vesta: Testing the Protoplanetary Paradigm. Science, 33, 684–686.

Simon, S.B., Davis, A.M., Grossman, L., and McKeegan, K.D. (2002) A hibonite-corundum inclusion from Murchison: A first-generation condensate from the solar nebula. Meteoritics & Planetary Science, 37, 533–548.

Stolper, E. (1975) Petrogenesis of eucrite, howardite and diogenite meteorites. Nature, 258, 220–222.

Sutherland, F.L., Hoskin, P.W.O., Fanning, C.M., and Coenraads, R.R. (1998) Models of corundum origin from alkali basaltic terrains: a reappraisal. Contributions to Mineralogy and Petrology, 133, 356–372.

Takigawa, A., Stroud, R.M., Nittler, L.R., Alexander, C.M.O.D., and Miyake, A. (2018) High-temperature dust condensation around an AGB star: Evidence from a highly pristine presolar corundum. The Astrophysical Journal Letters, 862, L13.

Wadhwa, M., Amelin, Y., Bogdanovski, O., Shukolyukov, A., Lugmair, G.W., and Janney, P. (2009) Ancient relative and absolute ages for a basaltic meteorite: implications for timescales of planetesimal accretion and differentiation. Geochimica et Cosmochimica Acta, 73, 5189–5201.

Yang, J., Zhang, C., Miyahara, M., Tang, X., Gu, L., and Lin, Y. (2019) Evidence for early impact on a hot differentiated planetesimal from Al-rich micro-inclusions in ungrouped achondrite Northwest Africa 7325. Geochimica et Cosmochimica Acta, 258, 310–335.

Zhang, A.C., Hsu, W.B., Li, X.H., Ming, H.L., Li, Q.L., Liu, Y., and Tang, G.Q. (2011) Impact melting of Dhofar 458 lunar meteorite: Evidence from polycrystalline texture and decomposition of zircon. Meteoritics & Planetary Science, 46, 103–115.

Zhang, A.C., Ma, C., Sakamoto, N., Wang, R.C., Hsu, W.B., and Yurimoto, H. (2015) Mineralogical anatomy and implications of a Ti-Sc-rich ultra-refractory inclusion from Sayh al Uhaymir 290 CH3 chondrite. Geochimica et Cosmochimica Acta, 163, 27–39.

Zhang, A.C., Kawasaki, N., Bao, H., Liu, J., Qin, L., Kuroda, M., Gao, J.F., Chen, L.H., He, Y., Sakamoto, N., and Yurimoto, H. (2020) Evidence of metasomatism in the interior of Vesta. Nature Communications, 11, 1289. Doi: 10.1038/s41467-020-15049-7.

Zinner, E. (2014) Presolar grains. In Treatise on Geochemistry 2nd edition, Volume 1 (edited by Davis A. M.). Pp. 181–214.

Zolensky, M.E., Weisberg, M.K., Buchanan, P.C., and Mittlefehldt, D.W. (1996) Mineralogy of carbonaceous chondrite clasts in HED achondrites and the Moon. Meteoritics & Planetary Science, 31, 518–537.

Zuber, M.T., McSween, H.Y., Binzel, R.P., Elkins-Tanton, L.T., Konopliv, A.S., Pieters, C.M., and Smith, D.E. (2011) Origin, internal structure and evolution of 4 Vesta. Space Science Review, 163, 77–93.

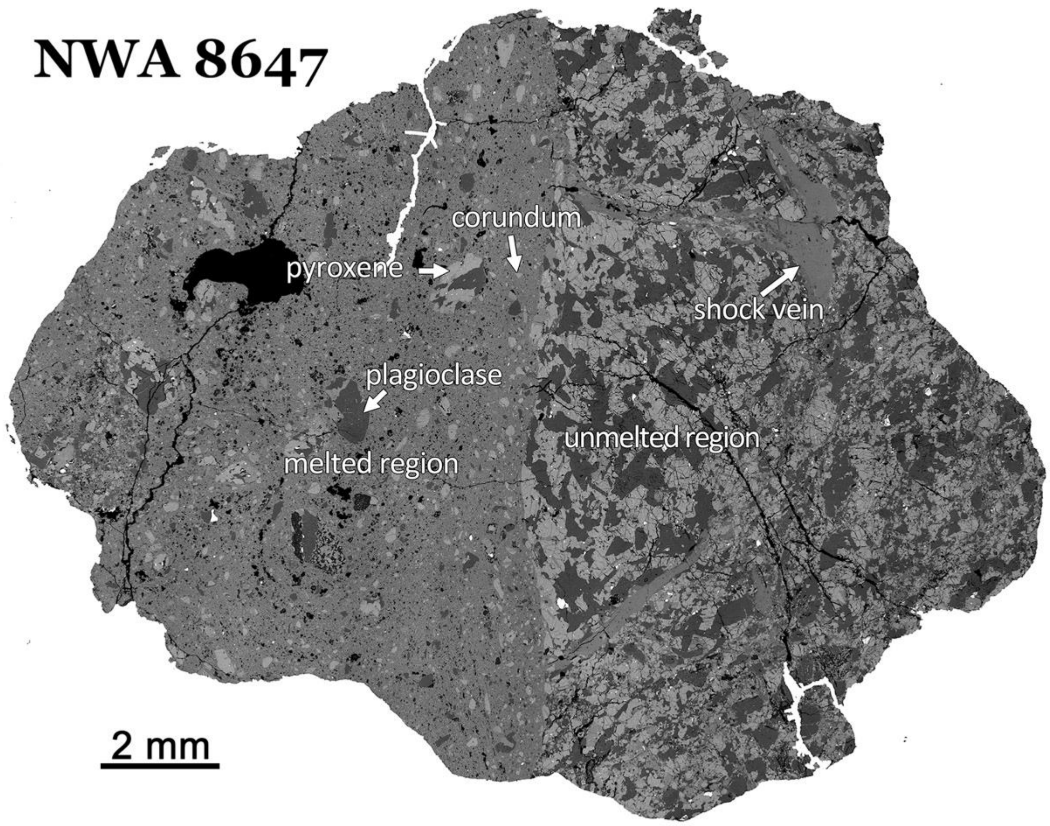

Figure 1. Mosaic backscattered electron image of the section of NWA 8647. The left side shown in this image was largely melted and recrystallized. However, the right side was unmelted but contains shock-induced melt veins.

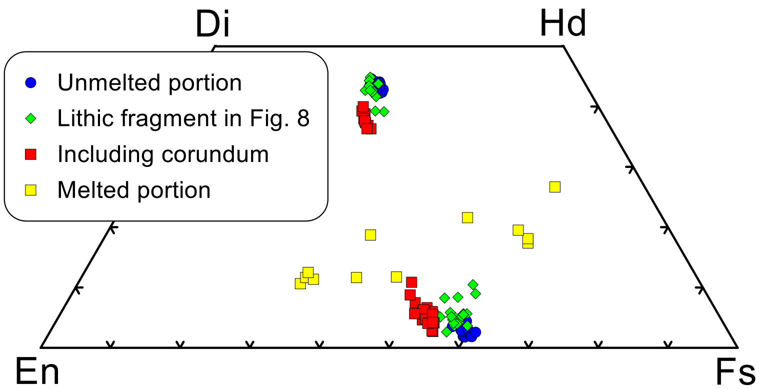

Figure 2. Pyroxene quadrilateral diagram showing the compositional variation of pyroxenes in NWA 8647. Blue circles represent compositions of the coarse-grained pyroxenes in the unmelted portion. Green diamonds represent compositions of the polycrystalline pyroxenes in the lithic fragment shown in Fig. 8. Red squares are compositions of the pyroxenes in the fragment hosting the corundum grain. Yellow squares represent compositions of fine-grained pyroxenes in the melted and recrystallized region.

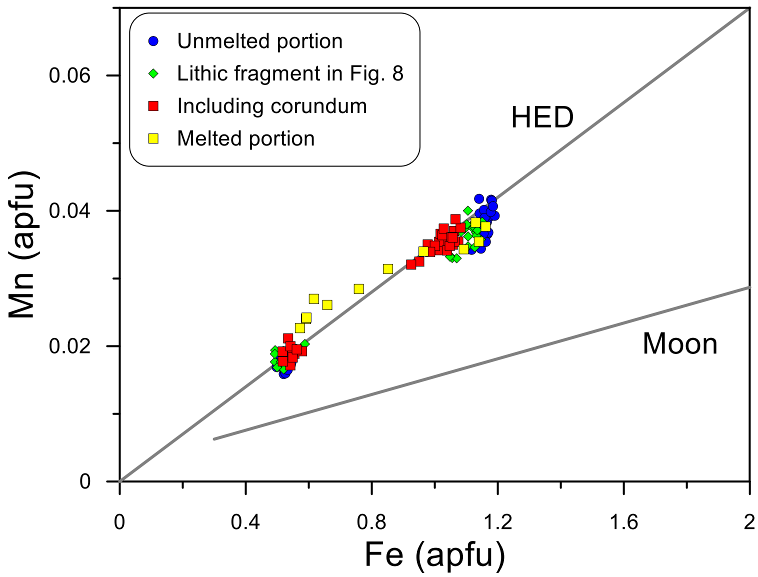

Figure 3. Fe and Mn compositions of pyroxene in NWA 8647. The trend lines of HED and Moon are adopted from Papike et al. (2003). The symbols in this figure are same as those in Fig. 2.

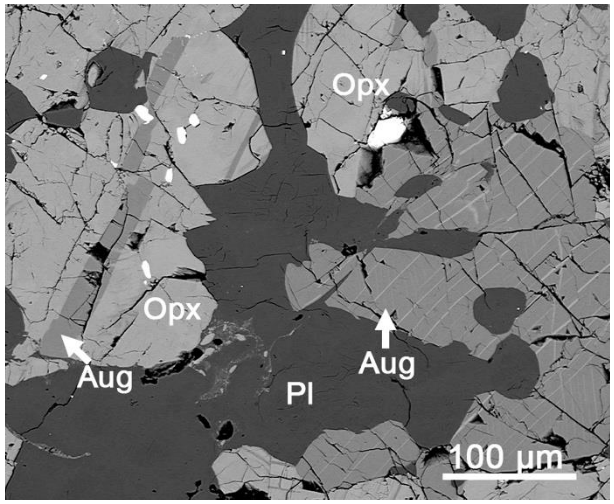

Figure 4. Typical area from the unmelted region in NWA 8647 showing the exsolution texture of pyroxene. Opx: orthopyroxene; Aug: augite; Pl: plagioclase.

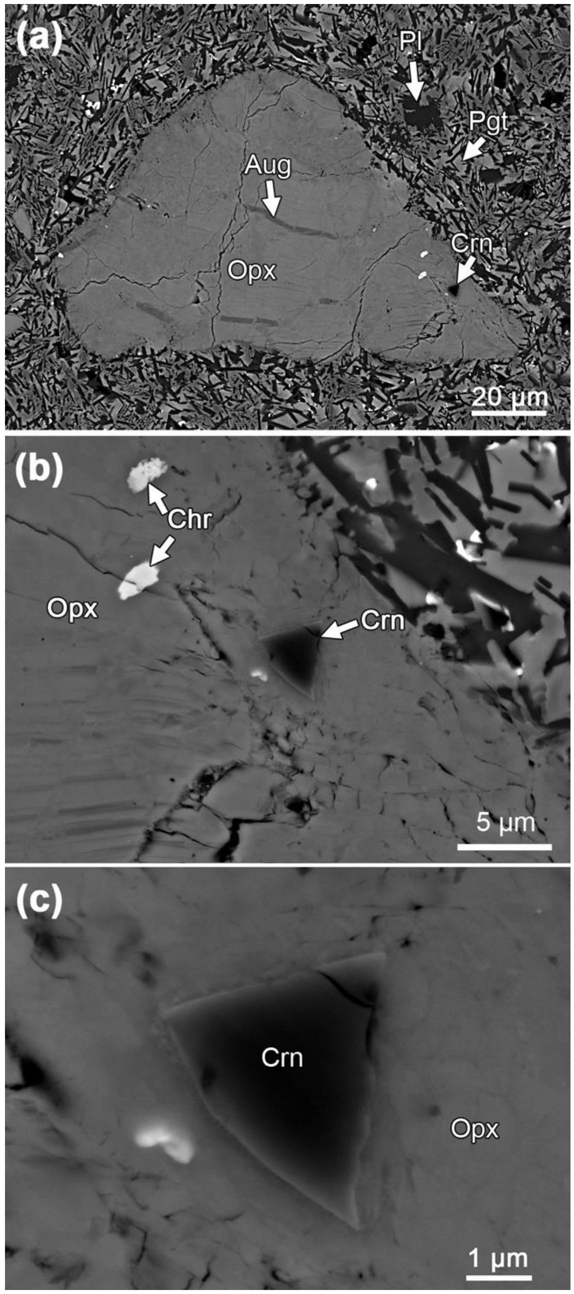

Figure 5. BSE image of the pyroxene grain containing corundum (a) and the zoom-in images (b–c) with various magnifications of the local regions containing the corundum grain. In (b), two fine-grained chromite grains are also present and the upper one shows a polycrystalline texture. Pgt: pigeonite; Aug: augite; Opx: orthopyroxene; Pl: plagioclase; Crn: corundum; Chr: chromite.

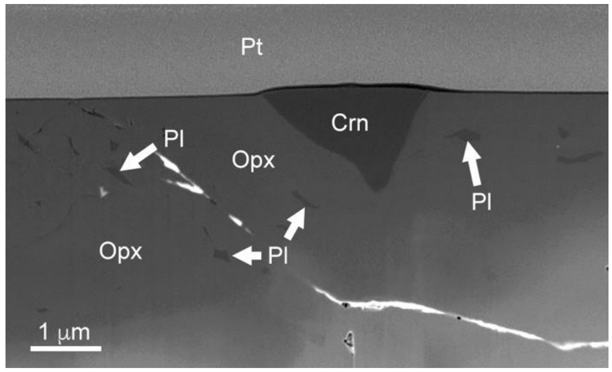

Figure 6. Secondary electron image of the FIB section showing the relationship between corundum and surrounding silicate minerals. Crn: corundum; Opx: orthopyroxene; Pl: plagioclase; Pt: Pt metal.

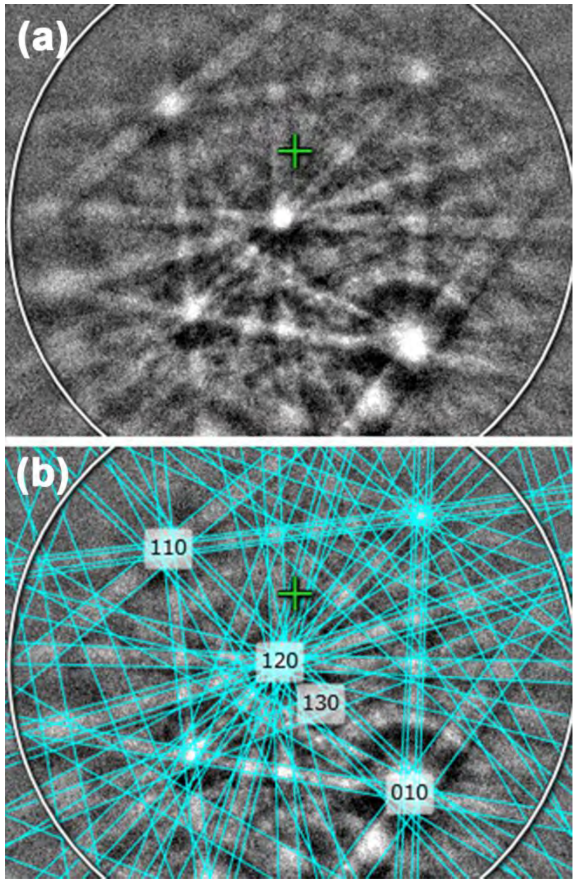

Figure 7. EBSD pattern (a) of the labelled corundum crystal in Fig. 5b and the pattern (b) indexed with the trigonal $R\overline{3}c$ structure (MAD=0.21).

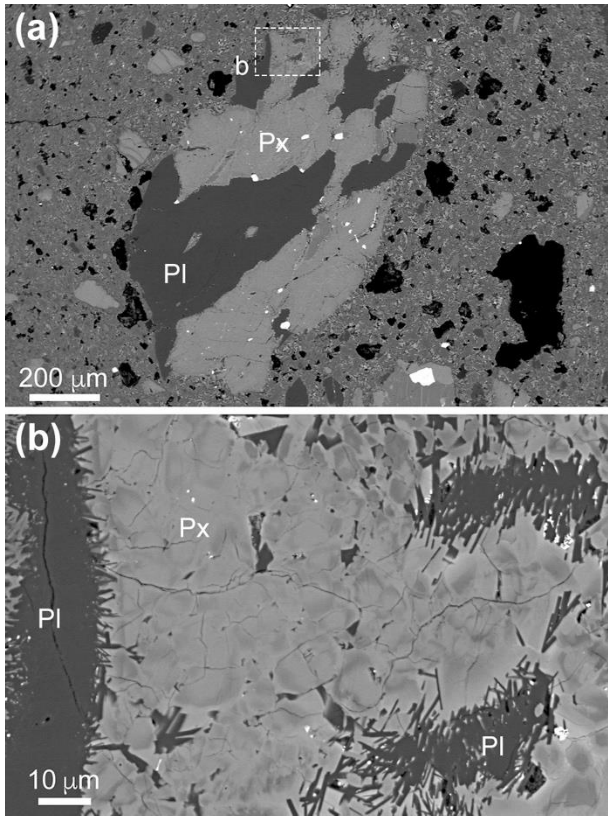

Figure 8. (a) Backscattered electron image of relict lithic fragment in the melted region of NWA 8647. The white box indicates the location of (b). (b) zoomed-in image of a typical region from the upper part of (a) showing polycrystalline pyroxene. Note that plagioclase grains in (b) have a high length/width ratio, indicating rapid crystallization from melt. Px: pyroxene; Pl: plagioclase.